The interior of a binary black hole merger

Daniel Pook-Kolb,[1,2] Ofek Birnholtz,[3] Badri Krishnan,[1,2] and Erik Schnetter[4,5,6]

[1]*Max-Planck-Institut für Gravitationsphysik (Albert Einstein Institute), Callinstr. 38, 30167 Hannover, Germany*
[2]*Leibniz Universität Hannover, 30167 Hannover, Germany*
[3]*Center for Computational Relativity and Gravitation, Rochester Institute of Technology, 170 Lomb Memorial Drive, Rochester, New York 14623, USA*
[4]*Perimeter Institute for Theoretical Physics, Waterloo, ON N2L 2Y5, Canada*
[5]*Physics & Astronomy Department, University of Waterloo, Waterloo, ON N2L 3G1, Canada*
[6]*Center for Computation & Technology, Louisiana State University, Baton Rouge, LA 70803, USA*

(Dated: 2019-03-12)

We find strong numerical evidence for a new phenomenon in a binary black hole spacetime, namely the merger of marginally outer trapped surfaces (MOTSs). We show that the MOTS associated with the final black hole merges with the two initially disjoint surfaces associated with the two initial black holes. This yields a connected sequence of MOTSs interpolating between the initial and final state all the way through the non-linear binary black hole merger process. This now allows us to track physical quantities (such as mass, angular momentum, higher multipoles, and fluxes) across the merger, which can be potentially compared with the gravitational wave signal in the wave-zone, and with observations by gravitational wave detectors. This also suggests a possibility of proving the Penrose inequality for generic astrophysical binary back hole configurations.

The standard picture of the merger of two black holes (BHs) is often visualized by an event horizon (EH), the boundary of the portion of spacetime causally disconnected from far away observers. An example of this is [38], showing the well known "pair of pants" picture of the EH. However, EHs are not suitable for extracting quantities of physical interest and track them all the way through the merger in quantitative studies. In perturbative regimes or in cases when the end state of the EH is known, it is sometimes possible to use EHs to calculate mass, angular momentum, energy fluxes etc. [27], but this does not carry over to non-perturbative situations (such as during a binary black hole (BBH) merger) [11, 13, 24, 28].

It is much more satisfactory, both for conceptual and practical reasons, to use instead marginally trapped surfaces. The notion of a trapped surface was first introduced by Penrose for the singularity theorems [40]. Let S be a closed 2-surface with in- and out-going future-directed null normals n^a and ℓ^a respectively. Let $\Theta_{(\ell)}$ and $\Theta_{(n)}$ be the expansions of ℓ^a and n^a respectively. Trapped surfaces have $\Theta_{(\ell)}$ and $\Theta_{(n)}$ negative, while a marginally outer trapped surface (MOTS) has $\Theta_{(\ell)} = 0$ (with no restriction on $\Theta_{(n)}$). The outermost MOTS on a given Cauchy surface, known as an apparent horizon (AH), has been used to locate BHs even in the earliest numerical BH simulations (see e.g. [45]). The presence of a trapped surface in a spacetime shows the presence of a singularity and an EH. MOTSs were thus used as proxies for EHs (which are much harder to locate numerically). Over the last two decades, however, it has become clear that MOTSs are much better behaved than previously expected. The world tube traced out by a MOTS during time evolution can be used to study energy fluxes, the evolution of mass, angular momentum and higher multipole moments [7, 22, 26, 32, 44]). The world tube can be used as an inner boundary for Hamiltonian calculations, and the laws of BH mechanics hold [11, 13, 16, 25, 29, 31, 33]. In stationary spacetimes and in perturbative settings, these calculations coincide with expectations from EHs, but this framework works more generally.

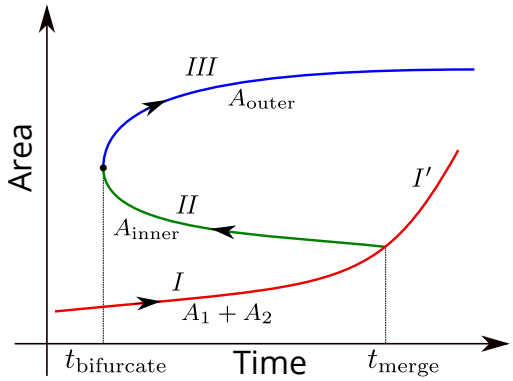

FIG. 1: The scenario for the merger of two separated marginal surfaces to yield a single final BH and the monotonicity of area increase during the merger along the directed path.

There remains, however, a significant gap in our understanding. For a BBH merger it is routine to compute physical quantities for either the two separate initial BHs or for the common final BH. It is not clear, however, if there should exist a relationship between the two regimes separated by the merger. Neither is it known whether there is a connected sequence of MOTSs which takes us from the two separated individual MOTSs to the final one. The existence of such a connected sequence would allow the possibility of tracing physical quantities all the way through the dynamical and non-linear merger process. These predictions

could potentially be compared with calculations of gravitational wave (GW) signals in the wave-zone and eventually with observations of GWs, thus offering a unique probe of dynamical and non-linear gravity.

Another motivation for studying this is related to cosmic censorship and the Penrose inequality (PI). In 1973, Roger Penrose proposed an inequality relating the area A of a BH horizon to the spacetime's total ADM mass M_{ADM} [41]:

$$A \leq 16\pi M_{ADM}^2 \,. \tag{1}$$

As originally formulated by Penrose, this inequality applies to a marginally trapped surface S formed during gravitational collapse and it brings together three of the most important results of general relativity: a) the area increase law for EHs which relies on cosmic censorship, b) the question of the final state of gravitational collapse, i.e. the BH uniqueness theorems, and finally c) the positivity of outgoing GW flux at infinity. The most uncertain of these is cosmic censorship. An alternate means of establishing the PI (without using the EH) would thus provide important support for cosmic censorship. Thus far, the PI has been established rigorously for time symmetric initial data for an arbitrary number of BHs [17, 18, 30] (see [2, 19, 35, 37] for some alternate approaches, and [36] for a review). Note also that there are examples of AHs which violate the inequality [12].

For a BBH system, the PI implies

$$A_1 + A_2 \leq 16\pi M_{ADM}^2 \,, \tag{2}$$

where $A_{1,2}$ are the initial areas of the two individual BHs, taken to be two disjoint MOTSs $\mathcal{S}_1$ and $\mathcal{S}_2$. Let $\mathcal{S}_f$ be the final MOTS with area A_f. In this paper, we provide evidence for a very different way of tackling the PI, namely by following the time evolution of $\mathcal{S}_{1,2}$. The goal is to establish that $A_1 + A_2 \leq A_f$. At late times when the BH has reached equilibrium, cross-sections of the event horizon are also marginally trapped surfaces. Thus, we would like to establish that there is a connected sequence of marginal surfaces, with monotonically increasing area, which takes us from $\mathcal{S}_1$ and $\mathcal{S}_2$ to $\mathcal{S}_f$.

Our proposed scenario is sketched in Fig. 1. We start with the two BHs far apart, represented by the MOTSs $\mathcal{S}_1$ and $\mathcal{S}_2$, and track their areas A_1 and A_2, respectively. The branch I and I' (red) show $A_1 + A_2$ which is always increasing. The common horizon is formed with a bifurcation into inner and outer portions $\mathcal{S}_{\rm inner}$ and $\mathcal{S}_{\rm outer}$, respectively, at the time $t_{\rm bifurcate}$. $\mathcal{S}_{\rm inner}$ generates the branch II (green), which decreases in area and eventually merges with I at time $t_{\rm merge}$ (which demarcates I and I'). Segment III (blue) is traced out by the AH which has increasing area and asymptotes to a final Schwarzschild or Kerr horizon. The required sequence of MOTSs is then $I + II + III$; if we have monotonic area increase along this sequence, the PI will hold (segment II is traversed backwards in time). Note, however, that the portion I' is not part of this sequence and the MOTSs in this part might in fact end up with a larger area than the AH.

There are several subtle points regarding this scenario and its regime of validity (we show that it is in fact *not* true in general for time-symmetric initial data). Our goal in this paper is to provide support for this scenario for astrophysical initial configurations corresponding to the head-on collision of two non-spinning BHs. We remark that even for a single BH—while we have evidence from numerical and analytic calculations that the end state of branch III must be a Kerr BH —this is not yet mathematically established in the full non-linear theory. This work does not add anything in that direction. However, it does suggest a mechanism of extending this result, if it holds, to multiple BHs.

Preliminaries.– We recall here two technical details which will be important below. The first is the stability operator for a MOTS which determines its behavior under deformations [4, 5, 14, 42]. If r^a is a unit spacelike normal to S, and f a function on S, then we can vary S along fr^a and compute the expansion for the deformed surfaces. Differentiation of the expansion then leads to the variation of the outgoing expansion $\Theta_{(\ell)}$, denoted $\delta_{fr}\Theta_{(\ell)}$. The stability operator L acting on a function f is defined as

$$L[f] := \delta_{fr}\Theta_{(\ell)} \,. \tag{3}$$

In general L is a linear elliptic operator but is not necessarily self-adjoint. Nevertheless, its principle eigenvalue Λ_0, i.e. the eigenvalue with lowest real part is real. It can be shown that the invertibility of L guarantees that S evolves smoothly at least locally in time (as long as L remains invertible). In particular, if $\Lambda_0 > 0$, stable time evolution is guaranteed locally in time since then no eigenvalue of L vanishes. In case $\Lambda_0 < 0$, as will happen here, then we need to consider the next eigenvalue Λ_1: as long as its real part is positive then S evolves smoothly. If a MOTS has $\Lambda_0 > 0$, it generically traces out a spacelike surface and has increasing area. In general the world tubes can be null, timelike or of mixed signature and can have decreasing area [8–11, 15, 16].

The other important technical tool is a new method for locating MOTSs numerically which is capable of finding even very highly distorted MOTSs [42]. This is a modification of the commonly used algorithm known as AHFinderDirect [46]. It was previously validated for sequences of time-symmetric initial data sets, and is here applied during a time evolution. The software [43] has since been modified and can now be applied to non time-symmetric cases as well. It is presently restricted to axisymmetry, but no in-principle difficulties are foreseen for general cases.

We use the Einstein toolkit [23, 34] infrastructure for our calculations. We set up initial conditions via the two-puncture single-domain method [6] and enforce axisymmetry by the *Cartoon* method [1]. We solve the Einstein equations in the BSSN formulation as in [21], using a $1 + \log$ slicing and a Γ-driver shift condition, with details of our initial and gauge conditions as described in [47].

We use fourth order finite differencing on a uniform grid spanning $[0, 10] \times [0, 0] \times [-10, 10]$ and a fourth order

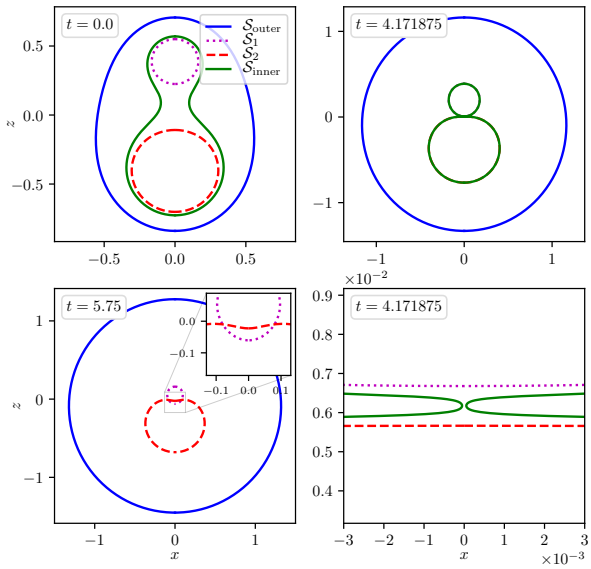

FIG. 2: The shapes of the horizons at various times in the simulation. Details in text.

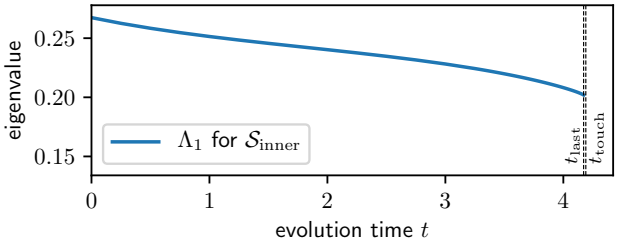

FIG. 3: The stability parameter for $\mathcal{S}_{\rm inner}$ as a function of time. The curve terminates at $t_{\rm last}$, the last time that we locate $\mathcal{S}_{\rm inner}$. The time $t_{\rm touch}$ when $\mathcal{S}_{1,2}$ touch is just a little bit later, but not visually distinguishable from $t_{\rm last}$.

Runge-Kutta time integrator. Most calculations shown here were performed with a resolution of $h = 1/256$, and some with $h = 1/512$ to resolve details. All parameter files are available in the repository [43].

The merger of the inner horizons.– We consider head-on collisions of non-spinning BHs. We shall always use time-symmetric Brill-Lindquist (BL) initial data [20], representing a BBH system at a moment of time-symmetry. The bare masses of the two BHs are denoted (m_1, m_2) and d_0 is the initial separation. While the PI is known to physically hold in BL data, no such time symmetry is expected to occur in any astrophysical situation in our universe. Time symmetry implies that the two BHs approach each other and merge also under time reversal. Furthermore, the incoming radiation at past null-infinity mirrors the outgoing radiation at future null-infinity. This non-physical, exceptional aspect of BL data at finite d_0 will be important later.

Some partial results on the behavior of $\mathcal{S}_{\rm inner}$ were

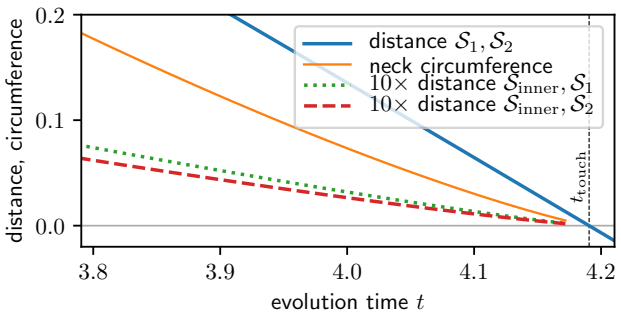

FIG. 4: Different measures showing the merger $\mathcal{S}_{1,2,\rm inner}$.

known previously [26, 44]: $\mathcal{S}_{\rm inner}$ decreases rapidly in area initially and becomes increasingly distorted as it approaches $\mathcal{S}_1$ and $\mathcal{S}_2$. With our new horizon finder, we are able to track $\mathcal{S}_{\rm inner}$ almost up to the merger point. We present our results first for a particular initial configuration $d_0 = 0.75$, $m_1 = 0.5$, and $m_2 = 0.8$. For this starting separation, the common horizon has already formed and thus the AH is always disconnected from any of the inner horizons. This aspect will not be important for the moment, and we wish to focus only on the inner horizons here. The shapes of the various marginal surfaces at selected instants of time are shown in Fig. 2. The top-left panel shows the initial configuration with the AH already formed and $\mathcal{S}_{\rm inner}$ fairly distorted. The bottom-left panel shows the horizons at a late time when $\mathcal{S}_{\rm inner}$ no longer exists, and $\mathcal{S}_1$ and $\mathcal{S}_2$ penetrate each other; this feature was first observed in [39]; see also [3].

We are able to track $\mathcal{S}_{\rm inner}$ much further until it almost coincides with $\mathcal{S}_{1,2}$. The top-right panel shows the MOTSs at the last time for which we are able to locate $\mathcal{S}_{\rm inner}$, namely $t_{\rm last} = 4.171875$. This is just a few time steps before the time at which $\mathcal{S}_{1,2}$ touch each other: $t_{\rm touch} = 4.190585$. The bottom right panel shows a close-up of the neck of $\mathcal{S}_{\rm inner}$, which is very close to pinching off (note the much smaller length scale of this panel). We lose track of $\mathcal{S}_{\rm inner}$ because of the extremely narrow neck which requires a large number of collocation points to resolve. The numerical difficulties very close to the merger are primarily related to the choice of a reference surface used to construct a local coordinate system in our numerical method [42]. Due to the very high curvature of the MOTS at its neck, the numerics becomes very sensitive to the choice of the reference surface. We expect $\mathcal{S}_{\rm inner}$ should still exist for a few more time steps. This is confirmed by the stability parameter of $\mathcal{S}_{\rm inner}$, i.e. the second eigenvalue Λ_1 of the stability operator shown in Fig. 3. In this case the operator is self-adjoint and Λ_1 is real. We see that Λ_1 is positive, very far from vanishing and shows no large variations.

Fig. 4 shows various quantities which must all vanish at the point of merger. First, it shows the proper distance between $\mathcal{S}_1$ and $\mathcal{S}_2$ measured at facing points along the

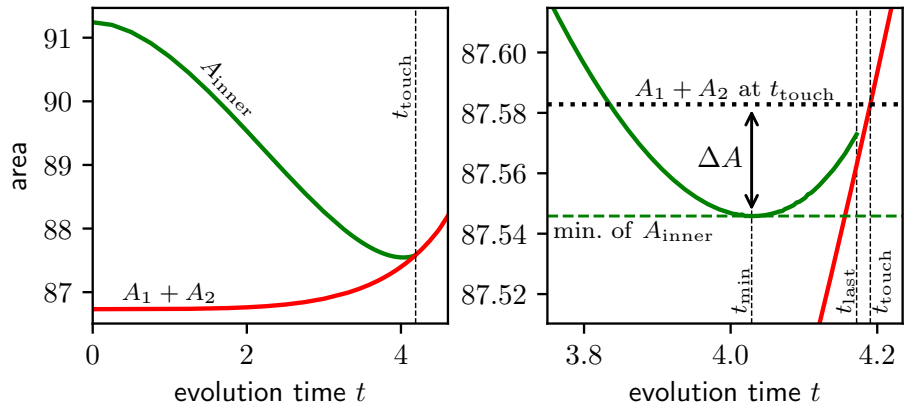

FIG. 5: The area of the inner common MOTS (green) and the sum of the areas of the individual MOTSs (red) along the evolution time. *Left*: the full evolution. *Right*: a zoom-in on the times around the minimum of $A_{\rm inner}$ ($t_{\rm min}$) and the touching of the two individual MOTSs ($t_{\rm touch}$). The curve for $A_{\rm inner}$ (green) terminates at $t_{\rm last}$.

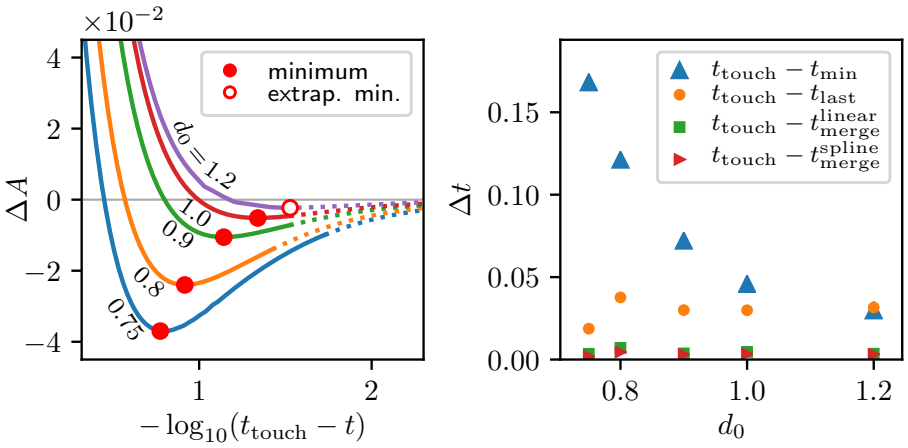

FIG. 6: *Left*: The behavior of the area of $\mathcal{S}_{\rm inner}$, approaching $t_{\rm touch}$, for different initial separations d_0. ΔA is computed with the final area assumed to be $A_1 + A_2$ at $t_{\rm touch}$. *Right*: The convergence of the times $t_{\rm touch}$ and $t_{\rm min}$ at large d_0.

z-axis. This distance crosses 0 when both MOTSs touch. Then we plot the proper circumference of the neck of $\mathcal{S}_{\rm inner}$, the proper distance between $\mathcal{S}_{1,2}$ and $\mathcal{S}_{\rm inner}$ along the z-axis (the latter distances are scaled up by a factor of 10 to be properly visible on this plot). All of these quantities indicate that $\mathcal{S}_{\rm inner}$ pinches off when $\mathcal{S}_{1,2}$ touch. We thus postulate that the time $t_{\rm touch}$ when $\mathcal{S}_{1,2}$ touch is the same as the time $t_{\rm merge}$ when $\mathcal{S}_{\rm inner}$ merges with $\mathcal{S}_{1,2}$. This is quantified below.

The area increase law.– The area of $\mathcal{S}_{\rm inner}$ and the sum of the areas of $\mathcal{S}_{1,2}$ is shown in Fig. 5. The left panel shows the area starting right from $t = 0$, seemingly decreasing everywhere. However, the right panel shows a close-up near $t_{\rm touch}$ and surprisingly, it reveals a small area *increase* ΔA towards the end. Repeating the simulations for different d_0 (keeping $m_{1,2}$ fixed) shows that ΔA decreases with increasing d_0; see left panel of Fig. 6. For the simulations with $d_0 \geq 1.00$ the common horizon is not present in the initial configuration and it forms and bifurcates during the simulation.

The minima are marked with red dots in Fig. 6 (except for $d = 1.20$ where the minimum is obtained by extrapolation). It is clear that the area increase time, i.e. the time difference between $t_{\rm min}$ and $t_{\rm touch}$, also decreases with increasing d_0 and approaches zero as d_0 increases. This is also shown in the right panel of Fig. 6 (the blue triangles).

Since the area curves terminate at $t_{\rm last}$, we can extrapolate them to the point where the curves for $A_{\rm inner}$ and $A_1 + A_2$ meet, thereby providing an estimate for $t_{\rm merge}$. We use either a simple linear extrapolation or a spline extrapolation, which provide estimates $t^{\rm linear}_{\rm merge}$ and $t^{\rm spline}_{\rm merge}$ respectively. The right panel of Fig. 6 also shows these estimates (the green squares and the red triangles), confirming that these are consistent with $t_{\rm touch}$. Finally,

the orange circles show the difference $t_{\rm touch} - t_{\rm last}$ which indicates the numerical performance of the MOTS finder.

Conclusions.– We have studied the process by which two marginal surfaces merge to form a common final BH. This is similar to and complements the "pair of pants" picture of a BH merger using EHs. We have provided strong numerical evidence that there is a connected sequence of marginal surfaces in this process. This will potentially allow us to track physical quantities through the merger and to compare with results obtained from gravitational waveforms. Moreover, this scenario suggests a different way of attacking the Penrose inequality. For all "physical" initial configurations, we expect the area to be non-decreasing along the sequence, and the Penrose inequality is thus guaranteed to hold for all MOTSs on the sequence. A similar scenario should work for an arbitrary number of BHs as long as the mergers occur pairwise.

Acknowledgments.– We thank Lars Andersson, Abhay Ashtekar, Alex Nielsen, Jeff Winicour, and Jose-Luis Jaramillo for valuable discussions. O.B. acknowledges the National Science Foundation (NSF) for financial support from Grant No. PHY-1607520. The research was also supported by the Perimeter Institute for Theoretical Physics. Research at Perimeter Institute is supported by the Government of Canada through Industry Canada and by the Province of Ontario through the Ministry of Research and Innovation. Some calculations were performed on the *Niagara* cluster of the University of Toronto.

[1] M. Alcubierre, S. Brandt, B. Bruegmann, D. Holz, E. Seidel, R. Takahashi, and J. Thornburg. Symmetry without symmetry: Numerical simulation of axisymmetric systems using Cartesian grids. *Int. J. Mod. Phys.*, D10:273–290, 2001.

[2] S. Alexakis. The Penrose inequality on perturbations of the Schwarzschild exterior. 2015.

[3] L. Andersson, M. Mars, J. Metzger, and W. Simon. The time evolution of marginally trapped surfaces. *Classical and Quantum Gravity*, 26(8):085018, apr 2009.

[4] L. Andersson, M. Mars, and W. Simon. Local existence of dynamical and trapping horizons. *Phys.Rev.Lett.*, 95:111102, 2005.

[5] L. Andersson, M. Mars, and W. Simon. Stability of marginally outer trapped surfaces and existence of marginally outer trapped tubes. *Adv.Theor.Math.Phys.*, 12, 2008.

[6] M. Ansorg, B. Brügmann, and W. Tichy. A single-domain spectral method for black hole puncture data. *Phys. Rev. D*, 70:064011, 2004.

[7] A. Ashtekar, M. Campiglia, and S. Shah. Dynamical Black Holes: Approach to the Final State. *Phys. Rev.*, D88(6):064045, 2013.

[8] A. Ashtekar et al. Isolated horizons and their applications. *Phys. Rev. Lett.*, 85:3564–3567, 2000.

[9] A. Ashtekar and B. Krishnan. Dynamical horizons: Energy, angular momentum, fluxes and balance laws. *Phys. Rev. Lett.*, 89:261101, 2002.

[10] A. Ashtekar and B. Krishnan. Dynamical horizons and their properties. *Phys. Rev.*, D68:104030, 2003.

[11] A. Ashtekar and B. Krishnan. Isolated and dynamical horizons and their applications. *Living Rev. Rel.*, 7:10, 2004.

[12] I. Ben-Dov. The Penrose inequality and apparent horizons. *Phys. Rev.*, D70:124031, 2004.

[13] I. Booth. Black hole boundaries. *Can. J. Phys.*, 83:1073–1099, 2005.

[14] I. Booth and S. Fairhurst. Isolated, slowly evolving, and dynamical trapping horizons: geometry and mechanics from surface deformations. *Phys. Rev.*, D75:084019, 2007.

[15] R. Bousso and N. Engelhardt. New Area Law in General Relativity. *Phys. Rev. Lett.*, 115(8):081301, 2015.

[16] R. Bousso and N. Engelhardt. Proof of a New Area Law in General Relativity. *Phys. Rev.*, D92(4):044031, 2015.

[17] H. L. Bray. Proof of the riemannian penrose inequality using the positive mass theorem. *J. Differential Geom.*, 59(2):177–267, 10 2001.

[18] H. L. Bray and P. T. Chrusciel. The Penrose inequality. 2003.

[19] H. L. Bray and H. P. Roesch. Null Geometry and the Penrose Conjecture. 2017.

[20] D. R. Brill and R. W. Lindquist. Interaction energy in geometrostatics. *Phys. Rev.*, 131:471–476, 1963.

[21] J. D. Brown, P. Diener, O. Sarbach, E. Schnetter, and M. Tiglio. Turduckening black holes: an analytical and computational study. *Phys. Rev. D*, 79:044023, 2009.

[22] O. Dreyer, B. Krishnan, D. Shoemaker, and E. Schnetter. Introduction to Isolated Horizons in Numerical Relativity. *Phys. Rev.*, D67:024018, 2003.

[23] Einstein Toolkit: Open software for relativistic astrophysics. `http://einsteintoolkit.org/`.

[24] V. Faraoni and A. Prain. Understanding dynamical black hole apparent horizons. *Lecture Notes in Physics*, 907:1–199, 2015.

[25] E. Gourgoulhon and J. L. Jaramillo. A 3+1 perspective on null hypersurfaces and isolated horizons. *Phys. Rept.*, 423:159–294, 2006.

[26] A. Gupta, B. Krishnan, A. Nielsen, and E. Schnetter. Dynamics of marginally trapped surfaces in a binary black hole merger: Growth and approach to equilibrium. *Phys. Rev.*, D97(8):084028, 2018.

[27] S. W. Hawking and J. B. Hartle. Energy and angular momentum flow into a black hole. *Commun. Math. Phys.*, 27:283–290, 1972.

[28] S. A. Hayward. Black holes: New horizons. In *Recent developments in theoretical and experimental general relativity, gravitation and relativistic field theories. Proceedings, 9th Marcel Grossmann Meeting, MG'9, Rome, Italy, July 2-8, 2000. Pts. A-C*, pages 568–580, 2000.

[29] S. A. Hayward. Energy and entropy conservation for dynamical black holes. *Phys. Rev.*, D70:104027, 2004.

[30] G. Huisken and T. Ilmanen. The inverse mean curvature flow and the riemannian penrose inequality. *J. Differential Geom.*, 59(3):353–437, 11 2001.

[31] J. L. Jaramillo. An introduction to local Black Hole horizons in the 3+1 approach to General Relativity. *Int. J. Mod. Phys.*, D20:2169, 2011.

[32] B. Krishnan. Fundamental properties and applications of quasi-local black hole horizons. *Class. Quant. Grav.*,

25:114005, 2008.

[33] B. Krishnan. Quasi-local black hole horizons. In A. Ashtekar and V. Petkov, editors, *Springer Handbook of Spacetime*, pages 527–555. Springer-Verlag, 2014.

[34] F. Löffler, J. Faber, E. Bentivegna, T. Bode, P. Diener, R. Haas, I. Hinder, B. C. Mundim, C. D. Ott, E. Schnetter, G. Allen, M. Campanelli, and P. Laguna. The Einstein Toolkit: A Community Computational Infrastructure for Relativistic Astrophysics. *Class. Quantum Grav.*, 29(11):115001, 2012.

[35] M. Ludvigsen and J. A. G. Vickers. An inequality relating total mass and the area of a trapped surface in general relativity. *Journal of Physics A: Mathematical and General*, 16(14):3349–3353, oct 1983.

[36] M. Mars. Present status of the Penrose inequality. *Class. Quant. Grav.*, 26:193001, 2009.

[37] M. Mars and A. Soria. On the Penrose inequality along null hypersurfaces. *Class. Quant. Grav.*, 33(11):115019, 2016.

[38] R. A. Matzner, H. E. Seidel, S. L. Shapiro, L. Smarr, W. M. Suen, S. A. Teukolsky, and J. Winicour. Geometry of a black hole collision. *Science*, 270:941–947, 1995.

[39] P. Mösta, L. Andersson, J. Metzger, B. Szilágyi, and J. Winicour. The Merger of Small and Large Black Holes. *Class. Quant. Grav.*, 32(23):235003, 2015.

[40] R. Penrose. Gravitational collapse and space-time singularities. *Phys. Rev. Lett.*, 14:57–59, 1965.

[41] R. Penrose. Naked singularities. *Annals N. Y. Acad. Sci.*, 224:125–134, 1973.

[42] D. Pook-Kolb, O. Birnholtz, B. Krishnan, and E. Schnetter. Existence and stability of marginally trapped surfaces in black-hole spacetimes. *Phys. Rev. D*, 99:064005, Mar 2019.

[43] D. Pook-Kolb, O. Birnholtz, B. Krishnan, and E. Schnetter. MOTS Finder version 1.1, Mar. 2019. 10.5281/zenodo.2591105.

[44] E. Schnetter, B. Krishnan, and F. Beyer. Introduction to dynamical horizons in numerical relativity. *Phys. Rev.*, D74:024028, 2006.

[45] L. Smarr, A. Čadež, B. DeWitt, and K. Eppley. Collision of two black holes: Theoretical framework. *Phys. Rev. D*, 14:2443–2452, Nov 1976.

[46] J. Thornburg. Finding apparent horizons in numerical relativity. *Phys. Rev. D*, 54:4899–4918, 1996.

[47] B. Wardell, I. Hinder, and E. Bentivegna. Simulation of GW150914 binary black hole merger using the Einstein Toolkit, Sept. 2016.